Journal of Nuclear Materials 393 (2009) 61–66

Contents lists available at ScienceDirect

Journal of Nuclear Materials

journal homepage: www.elsevier.com/locate/jnucmat

Swelling and microstructure of austenitic stainless steel ChS-68 CW after high dose neutron irradiation

S.I. Porollo [a], Yu.V. Konobeev [a], F.A. Garner [b,*]

[a] State Scientific Center of Russian Federation – Institute of Physics and Power Engineering (IPPE), Obninsk, Kaluga Region, Russia
[b] Radiation Effects Consulting, 2003 Howell Avenue, Richland, WA 99354, USA

ARTICLE INFO

Article history:
Received 19 December 2008
Accepted 13 May 2009

ABSTRACT

Austenitic stainless steel ChS-68 serving as fuel pin cladding was irradiated in the 20% cold-worked condition in the BN-600 fast reactor in the range 56–84 dpa. This steel was developed to replace EI-847 which was limited by its insufficient resistance to void swelling. Comparison of swelling between EI-847 and ChS-68 under similar irradiation conditions showed improvement of the latter steel by an extended transient regime of an additional ~10 dpa. Concurrent with swelling was the development of a variety of phases. In the temperature range 430–460 °C where the temperature peak of swelling was located, the principal type of phase generated during irradiation was G-phase, with volume fraction increasing linearly with dose to ~0.5% at 84 dpa. While the onset of swelling is concurrent with formation of G-phase, the action of G-phase cannot be confidently ascribed to significant removal from solution of swelling-suppressive elements such as silicon. A plausible mechanism for the higher resistance to void swelling of ChS-68 as compared with EI-847 may be related to an observed higher stability of faulted dislocation loops in ChS-68 that impedes the formation of a glissile dislocation network. The higher level of boron in ChS-68 is thought to be one contributor that might play this role.

1. Introduction

Due to their unique physical–mechanical properties chromium–nickel stainless steels are widely applied in nuclear engineering. The austenitic stainless steel ChS-68 (0.06C–16Cr–15Ni–2Mo–2Mn–Ti–V–B) was developed in Bochvar's All-Russian Research Institute of Non-organic Materials as an alternative to the steel EI-847 (0.08C–16Cr–15Ni–3Mo–Nb) used earlier as the structural material of fuel pin cladding in Russian fast reactors. The use of cold-worked ChS-68 steel as cladding structural material led to an increase in fuel burn-up from 9 up to 11% h.a. (heavy atoms) in the BN-600 fast reactor as a result of the maximum dose accumulated by fuel pin cladding increasing from 70 to 94 dpa [1].

To increase fuel burn-up in the BN-600 reactor to $\geqslant$14% h.a., it will be necessary to develop a new cladding steel where accumulated doses for such burn-up will be $\geqslant$100 dpa. The experience of developing austenitic cladding steels for European fast reactors provides evidence that this task is difficult, but solvable [2].

For development of new steels capable of meeting such ambitious requirements, it is necessary to have a rather precise understanding of the processes occurring in cladding materials at high neutron doses. Changes in steel microstructure at high irradiation doses seem to be rather important in this regard, especially in the parametric dependence of phase stability and dislocation evolution.

In this paper, data are reported on void swelling, loop and dislocation microstructure and precipitate formation of 20% cold-worked ChS-68 fuel pin cladding taken from three subassemblies that were irradiated in BN-600 to different dose levels, reaching as high as 84 dpa. Preliminary results of investigation of the microstructure of this steel were presented at the Alushta conference for a smaller subset of irradiation conditions [3].

2. Materials and methods

Pin cladding tubes of 6.9 mm outer diameter and 0.4 mm wall thickness were fabricated from ChS-68 steel (20% CW). The fuel pins were irradiated in assemblies C-11, C-65, and C-63 of the BN-600 reactor inside of a hexagonal wrapper tubes made of EP-450 (13Cr–2Mo–Nb–V–B) ferritic–martensitic steel. The exact composition of the ChS-68 tubes in this study is unknown. It is certain that they lay within the specification, however.

The compositional specifications of ChS-68 cladding are shown in Table 1 together with the composition of stainless fuel pin cladding steels EI-847 and EP-172 used in Russia earlier as fuel pin cladding materials. Note that EP-172 is essentially a high boron variant of EI-847.

Irradiation conditions for fuel pins investigated in this study are shown in Table 2. To assure that representative behavior was

* Corresponding author. Tel.: +1 509 521 1633.
E-mail address: frank.garner@dslextreme.com (F.A. Garner).

0022-3115/$ - see front matter © 2009 Elsevier B.V. All rights reserved.
doi:10.1016/j.jnucmat.2009.05.005

Table 1
The chemical composition of cladding steels, wt%.

Chemical element	ChS-68	EI-847	EP-172
C	0.05 ÷ 0.08	0.04 ÷ 0.06	0.04 ÷ 0.07
Mn	1.3 ÷ 2.0	0.4 ÷ 0.8	0.5 ÷ 0.9
Si	0.3 ÷ 0.6	<0.4	0.3 ÷ 0.6
Cr	15.0 ÷ 16.5	15 ÷ 16	15 ÷ 16.5
Ni	14.0 ÷ 15.5	15 ÷ 16	14.5 ÷ 16.0
Mo	1.9 ÷ 2.5	2.7 ÷ 3.2	2.5 ÷ 3.0
V	0.1 ÷ 0.3	–	–
Nb	–	<0.9	0.35 ÷ 0.9
Ti	0.2 ÷ 0.5	–	–
B	0.002 ÷ 0.005	–	0.003 ÷ 0.008

Table 2
Irradiation conditions for fuel pins investigated.

Assembly	Maximum burn-up (% h.a.)	Maximum dose (dpa)	Maximum total neutron fluence (10^{27} n/m^2)
C-11	7.4	60	2.0
C-65	9.1	70	2.3
C-63	11.5	84	3.0

obtained in this study 2–3 adjacent pins were taken from each subassembly.

Axial profiles of dose and irradiation temperature are shown in Fig. 1 for one of the fuel pins removed from the C-63 assembly. For other pins the profiles are similar. Since the temperature of the cladding was decreasing during exposure due to fuel burn-up the temperature averaged over time is shown. At the upper end of these pins the difference of temperatures at the start and finish of irradiation equals approximately 50 °C. At lower elevations the temperature decrease is correspondingly lower.

Cladding segments with sizes of 15 mm × 4.5 mm were cut out from several sections along the pin length. In each case one of the cross sections corresponds to the position of maximum diametral strain. Microscopy specimens in the form of disks of 3 mm in diameter were prepared using a two-jet polishing 'TENUPOLE' device in such a manner that one could investigate the microstructure at the cladding at the mid-wall position. The microstructure was investigated using a JEM-100CX electron microscope equipped with a 'KEVEX' energy-dispersive X-ray micro-analyzer equipped with a lateral goniometer.

3. Results

The initial microstructure of ChS-68 steel from these cladding tubes consists of an austenitic matrix with occasional large (diameter up to 1 μm) metallurgical inclusions of type MX with number density of ~10^{17} m^{-3} (Fig. 2). These precipitates have an f.c.c-lattice of type TiC, in which a fraction of the Ti atoms are replaced by Mo atoms. Cold working to 20% resulted in the formation of twins and a dislocation cell structure with a mean dislocation density of ~10^{15} m^{-2}.

Typical axial profiles of pin cladding diametral strain for the three assemblies are shown in Fig. 3. A comparison of pin diametral strains with data on density change and swelling levels determined using electron microscopy revealed that the diametral strains are caused mainly by void swelling, i.e. the contribution of irradiation creep is negligible. Therefore, the variation in diametral strain is due primarily to the temperature and flux dependence of swelling. Note that the dose and dose rate at the top and bottom of the core are approximately 60% of that at the midplane.

The maximum diameter increase is located ~100 mm below the core center, where irradiation temperatures were in the range of

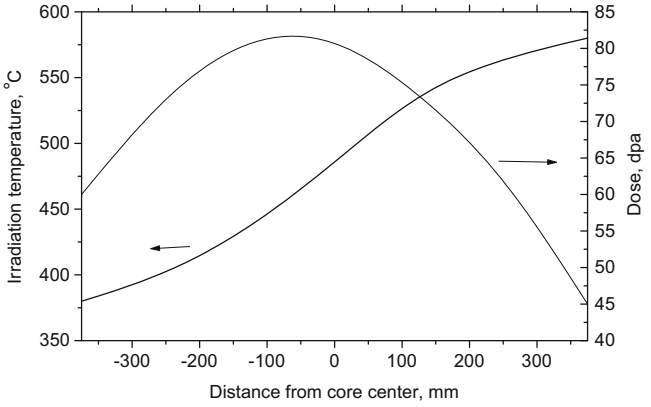

Fig. 1. Axial profiles of dose and irradiation temperature for pin # 18 of the C-63 subassembly.

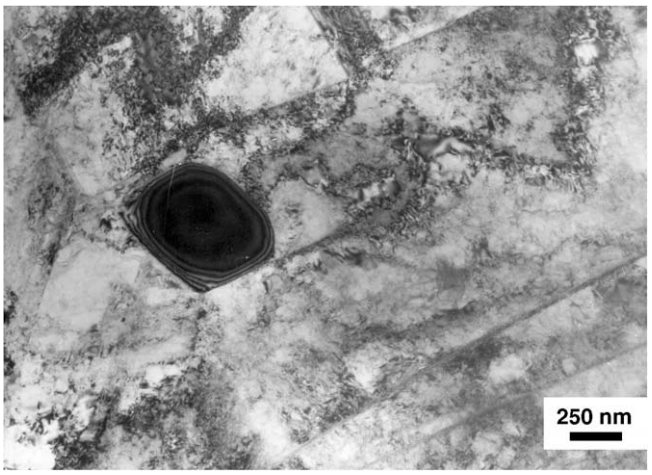

Fig. 2. Microstructure of non-irradiated ChS-68 (20% CW) steel showing a large inclusion.

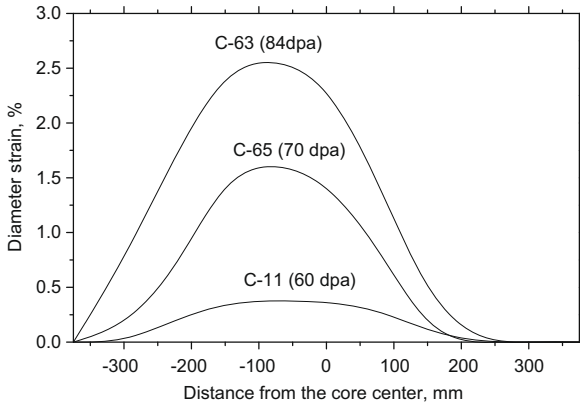

Fig. 3. Axial diametral strain profiles for typical fuel pins removed from the C-11, C-65, and C-63 assemblies.

430–460 °C. At temperatures above 550 °C swelling is rather low. The mean void diameter, void concentration and void volume fraction versus dose are shown in Figs. 4–6, derived from sections where the maximum diameter increase occurred. From these figures one can see that the swelling increased in the 56–84 dpa

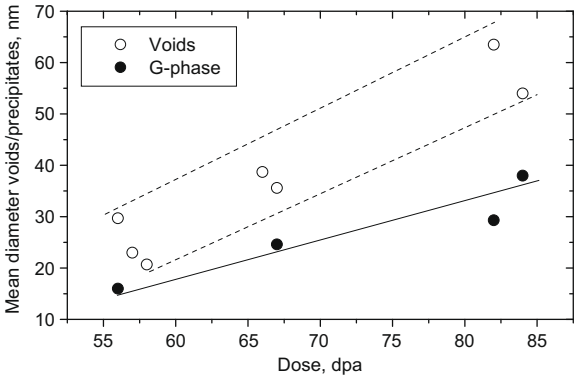

Fig. 4. Mean diameter of voids and G-phase precipitates versus dose in neutron irradiated ChS-68 CW steel ($T_{irr.}$ = 430–460 °C).

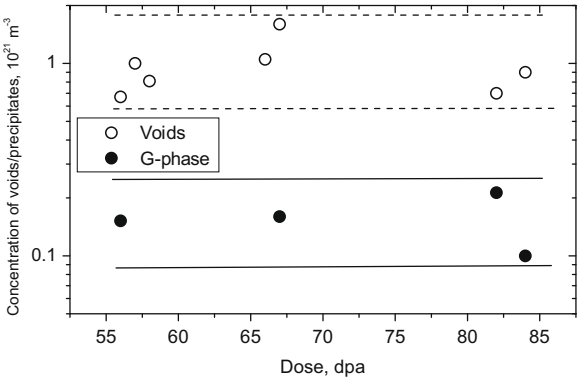

Fig. 5. Dose dependence of void and G-phase precipitate concentrations in neutron irradiated ChS-68 CW steel ($T_{irr.}$ = 430–460 °C).

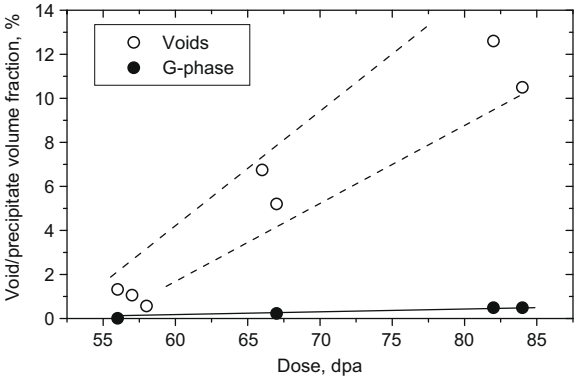

Fig. 6. Volume fraction of voids and G-phase precipitates as functions of dose in neutron irradiated ChS-68 CW steel ($T_{irr.}$ = 430–460 °C).

range arising primarily via increasing void size while the void concentration changed only slightly.

The spatial distribution of voids was often rather non-uniform. In bottom sections at lower temperature voids were seen to be absent in zones having high densities of deformation twins. In upper sections at $\geqslant$500 °C, voids were observed only in isolated regions, the volume of which decreased with increasing irradiation temperature. Additionally the void size distribution was often bimodal.

The dislocation structure of irradiated ChS-68 steel consisted of faulted Frank dislocation loops, perfect loops and dislocation segments. The dependence of mean diameter and concentration of Frank loops on irradiation temperature is shown in Fig. 7. The loop

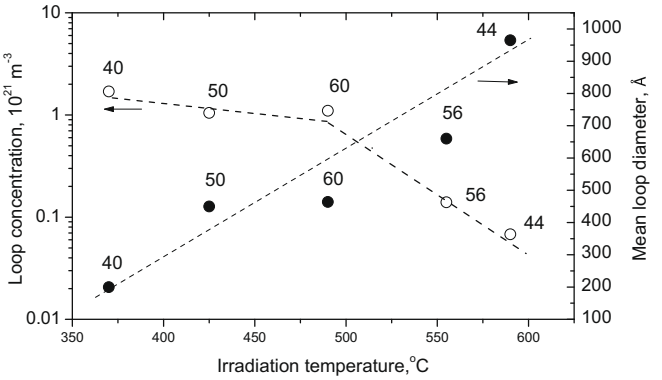

Fig. 7. Temperature dependence of mean diameter and concentration of Frank loops in neutron irradiated ChS-68 CW steel. Doses in dpa are indicated near the data points.

mean diameter increased with increasing temperature, and the loop concentration decreased correspondingly. The mean diameter of Frank loops also increased with increasing dose.

The dislocation network density depended slightly on irradiation temperature and dose and fell in the range of $(2 \div 6) \times 10^{14}$ m^{-2}. It should be noted that similar to the behavior of the voids, both Frank loops and dislocations were distributed rather non-uniformly at all irradiation temperatures. The most surprising observation, however, was that Frank loops still persisted to such high doses at this temperature. In all steels studied earlier Frank loops no longer existed at these doses.

Several types of precipitates were observed, including fine MX, γ′, G-phase, Laves, and carbides of type $M_{23}X_6$. A temperature–dose map of observed phases is shown in Fig. 8. It is seen that the principal type of precipitate in the range of temperatures at which the steel swells is G-phase. Some, but not all G-precipitates are adjacent to voids (Fig. 9). Dose dependencies of the mean diameter, concentration, volume fraction of G-phase precipitates are shown in Figs. 4–6. As seen from these figures, both the size of precipitate particles and their volume fraction increased almost linearly with increasing dose. The concentration of the precipitates changed slightly at doses ranging from 56 to 84 dpa. It should be noted that the dose dependencies of void and G-precipitate characteristics were similar although the void concentration is higher by one order of magnitude compared to the G-precipitate concentration.

Precipitates of γ′-phase were observed in ChS-68 CW steel at temperatures of 425 and 490 °C (at doses of 57 and 60 dpa, respectively) (Figs. 8 and 10). Their mean diameter increased from 9 to

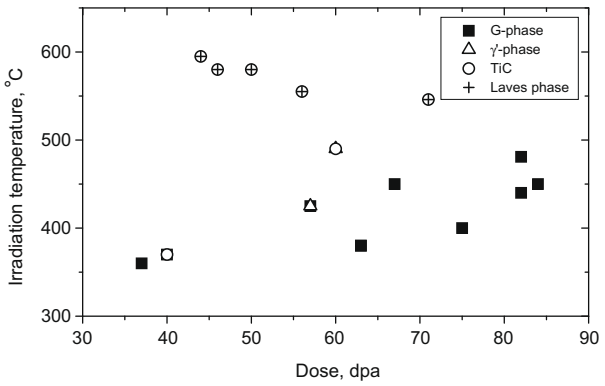

Fig. 8. Irradiation temperature–dose map of the secondary phase formation in neutron irradiated ChS-68 CW steel.

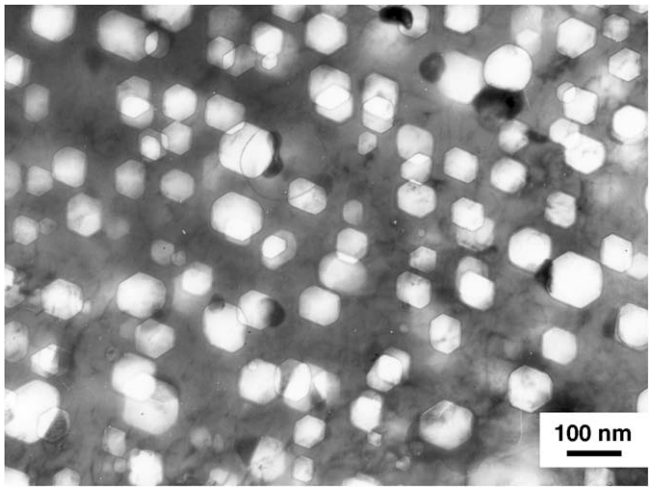

Fig. 9. Voids and G-precipitates in cold-worked ChS-68 CW steel at 440 °C and 84 dpa.

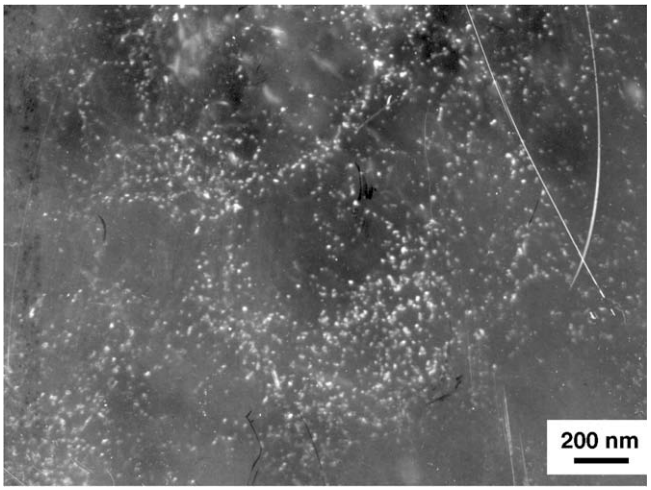

Fig. 11. Dark-field image of finely dispersed MX precipitates in cold-worked ChS-68 steel at 555 °C and 56 dpa.

17 nm, and their concentration fell from 2.4×10^{21} to 2.5×10^{20} m^{-3} as the temperature increased from 425 to 490 °C. The maximum volume fraction of γ′-phase was measured to be 0.17%.

With γ′-phase formation of 0.17% volume fraction and assuming a composition of Ni_3Si in a nominal 15 at% Ni-1.0 at% Si alloy, the concentration of Ni in the matrix drops from 15% to ~14.2%, while matrix Si drops to ~0.67 at.% or ~0.33 wt%. This is not a very large reduction in the swelling-suppressive element silicon.

Finely dispersed precipitates of type MX (Fig. 11) were formed under irradiation at temperatures above 500 °C. At the lowest dose of 40 dpa the formation of MX precipitates was also detected at 370 °C. Precipitate sizes fell in the 45–85 Å range and varied slightly with irradiation temperature. The spatial distribution of the MX precipitates was rather non-uniform within the grains, probably reflecting the original non-uniformity of dislocation structure in the cold-worked material.

Precipitates of Laves phase (Fig. 12) were formed at irradiation temperatures >500 °C. Some of the precipitates formed on larger precipitates of MX type while the rest were distributed inside of

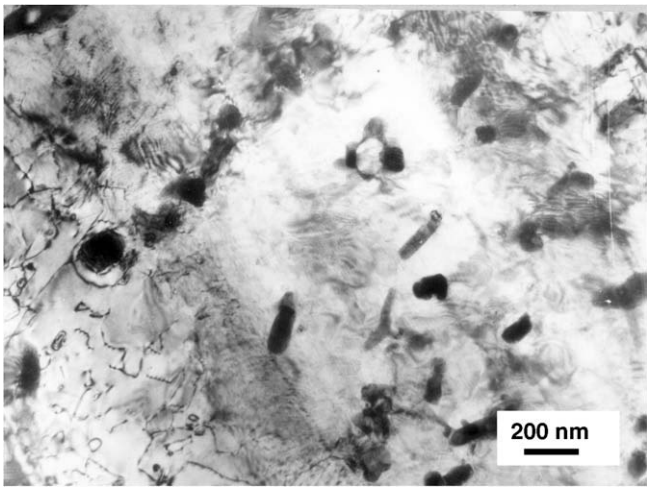

Fig. 12. Laves phase precipitates in cold-worked ChS-68 CW steel at 580 °C and 50 dpa.

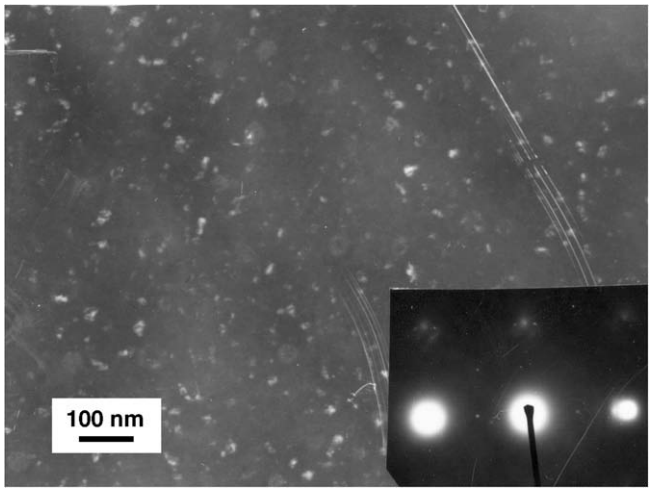

Fig. 10. Precipitates of γ′-phase imaged in dark-field in cold-worked ChS-68 steel at 425 °C and 57 dpa.

Fig. 13. Precipitates of type $M_{23}X_6$ on a grain boundary in cold-worked ChS-68 steel at 520 °C and 71 dpa.

the grains. The majority of the precipitates have an elongated form with maximum size of ~200 nm and a concentration reaching 1×10^{20} m^{-3}.

Intergranular precipitates of complex carbides of the type $M_{23}X_6$ (Fig. 13) were observed at temperatures above 500 °C. Their mean size and concentration increased with increasing irradiation temperature.

4. Discussion

It is seen from Figs. 1 and 3 that in the ChS-68 steel irradiated in BN-600 that the swelling peak is located in the 430–460 °C range. At these temperatures G-phase is the dominant type of precipitate (see Fig. 8). In Figs. 4–6, one can see that concentration of G-phase does not increase significantly with increasing dose. The volume fraction of G-precipitates increases with dose due to a nearly linear increase of the mean precipitate size. As it was noted previously, some G-phase precipitates are adjacent to voids. Since in the 430-460 °C range the void concentration exceeds the G-phase concentration by one order of magnitude, only one out of ten voids is adjacent to a precipitate. Voids adjacent to precipitates, as a rule, have larger sizes.

G-phase is a radiation-induced phase that does not normally form during thermal aging in steels like ChS-68. In stainless steels stabilized by titanium or niobium its nominal stoichiometric composition is $M_6Ni_{16}Si_6$ [4–6], i.e. this phase is enriched in Ni, Si, Ti or Nb and depletes the matrix of these elements. Note that there is no niobium in this steel. On the other hand, Si and Ti when in solid solution are well known to delay the onset of swelling, and reduction of matrix nickel content during precipitation is known to accelerate swelling [7,8]. Silicon in particular is known to be a particularly potent suppressor of swelling when in solution [9].

From this point of view the formation of G-phase is obviously an undesirable process. In the 50–84 dpa range the volume fraction of G-phase precipitates in ChS-68 CW steel increases linearly with dose and reaches a value of ~0.5%. Such linear dose dependence indicates that growth of this phase requires Ti and Si in sufficient concentration in the solid solution. From estimates based on the nominal stoichiometric composition and the G-phase lattice parameter of 1.12 nm it follows that at only ~0.1 wt% Ti and 0.06 wt% Si was removed from the solid solution into G-precipitates. Comparing these values with initial contents of Ti and Si in the steel (see Table 1), one can conclude that up to 84 dpa most of the silicon atoms (~85%) were still in solid solution. Titanium content in the solid solution was probably somewhat lower because some fraction of Ti atoms was in MX precipitates.

At irradiation temperatures above 500 °C, at which void concentrations are relatively low, intragranular fine dispersed MX carbides and Laves phase precipitates are the principal type of precipitates. These precipitates contain much less Si and Ni as compared with G-precipitates.

These results as observed in ChS-68 appear to be in conflict with the conventional wisdom that void swelling is accelerated by phases that remove swelling-suppressive elements. Obviously another factor is operating in this instance.

As it was noted earlier, ChS-68 austenitic steel was developed to replace EI-847 as the cladding material. Fig. 14 shows the dose dependencies of swelling of cold worked ChS-68 and EI-847 steels, obtained in electron microscopy investigations of fuel pin cladding irradiated in the BN-600 reactor [10]. Note that ChS-68 exhibits a longer transient regime of swelling compared to that of EI-847 (43 and 54 dpa, respectively) even though the swelling rates of the two steels are almost identical in the dose range investigated. The average swelling rate over this data set appears to be ~0.4%/dpa

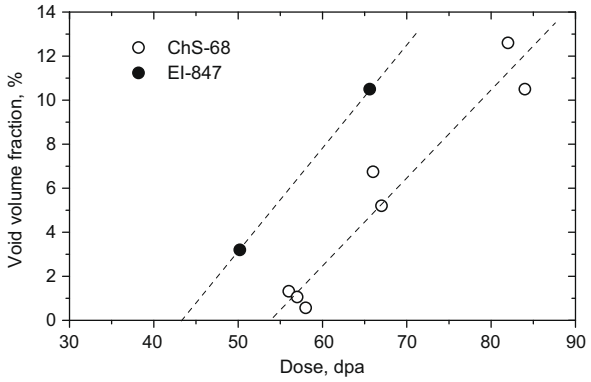

Fig. 14. Dose dependence of void volume fraction in neutron irradiated steels ChS-68 CW and EI-847 CW.

for both alloys, indicating that the terminal swelling rate of ~1%/dpa characteristic of austenitic alloys has not yet been reached.

Comparing chemical compositions of ChS-68 and EI-847 steels it is seen that their differences consist, primarily in that (1) Nb is the stabilizing chemical element in EI-847 steel while in ChS-68 steel Ti and V are the stabilizing elements with total content of Ti and V approximately equal to the Nb content of EI-847, and (2) B contents in ChS-68 steel are much higher in comparison with EI-847 steel.

How might such a difference of the chemical compositions result in an increase of cladding steel resistance to swelling? If we compare secondary phases in both steels at temperatures close to the peak swelling temperature, one notes that G-phase is the dominant type of precipitate and sometimes γ'-phase precipitates are observed. In contrast, in EI-847 at the same temperatures the principle phase is finely dispersed MX-precipitates and the amount of G-phase is insignificant. Such a difference of precipitates can be explained by the higher content of Si and Ti in ChS-68 steel. Nevertheless, based on the current results this difference in phases will not explain the ChS-68 behavior. Therefore, the higher resistance of ChS-68 steel to swelling as compared with EI-847 steel must be ascribed to another competing and perhaps more-dominant factor. One such factor may be the aforementioned higher stability of Frank loops observed in irradiated ChS-68 microstructure.

At irradiation temperatures close to the peak swelling temperature faulted dislocation loops were not observed in EI-847 steel at 50 dpa, while in ChS-68 steel they were observed at doses up to 82–84 dpa. This suggests that the dislocation structure evolution which involves stages of nucleation and growth of Frank loops, transformation of these loops into perfect loops, interaction between loops with dislocations and network formation may be happening more slowly in ChS-68 steel. It is well known that the highest swelling rate is observed after completion of the process of dislocation network formation [9].

The stability of faulted loops depends on their stacking fault energy. More stable loops resist unfaulting and interaction between the loops and dislocations, impeding and delaying dislocation network formation. Our opinion is the somewhat lower value of stacking fault energy in ChS-68 steel in comparison with EI-847 steel is due to its higher boron content since boron is known to have a strong effect on stacking fault energy [10]. Our conclusion follows from a comparison of dislocation structures of EI-847 and EP-172 stainless steels, with the latter differing from EI-847 steel only by a higher (up to 0.03 wt%) boron content. In EP-172 steel faulted loops were observed at higher doses as compared with EI-847 steel in side-by-side irradiations [11].

While this conclusion concerning stacking fault energy and boron content is not fully supported by the results of this report, suf-

ficient confidence has arisen from this study to address this possibility in future experiments.

5. Conclusions

Investigation of the microstructure of austenitic stainless steel ChS-68 irradiated in the 20% cold-worked condition in the BN-600 fast reactor in the range 56–84 dpa lead to the following conclusions:

1. After an incubation dose of ~54 dpa swelling of ChS-68 (20% CW) steel at 430–460 °C increases linearly with increasing dose with an average swelling rate of ~0.4%/dpa. Swelling at these irradiation conditions is caused mainly by void growth rather than by increased void nucleation.
2. In the temperature range 430–460 °C, where the temperature peak of swelling is located, the principle type of phase generated during irradiation in this steel is G-phase, with a volume fraction that is increasing linearly with dose, reaching ~0.5% at 84 dpa. At temperatures above 500 °C the swelling is low, and the principle intragranular precipitates are finely dispersed carbides of the MX type and Laves phase.
3. While it appears that the onset of swelling is either directly related to or coincident with formation of G-phase, its action can not be confidently ascribed to significant removal from solution of swelling-suppressive elements such as silicon. Apparently some other phenomenon must also be in operation.
4. In our opinion a plausible mechanism for the higher resistance to void swelling of ChS-68 (20% CW) as compared with that of EI-847 (20% CW) may be related to a higher stability of faulted dislocation loops that impedes the formation of a glissile dislocation network. The higher level of boron in ChS-68 is thought to be one contributor that might play this role.

Acknowledgement

This work was supported by the Russian Foundation for Basic Research under the Projects #07-02-01353 and #07-08-13642-ofi-c.

References

[1] B.A. Vasiljev, A.I. Zinovjev, A.I. Staroverov, V.V. Maltsev, A.N. Ogorodov, in: Proceedings of a Technical Committee Meeting on the Influence of High Dose Irradiation on Core Structural and Fuel Materials in Advanced Reactors, Obninsk, Russian Federation, IAEA-TECDOC-1039, 16–19 June 1997, p. 37.
[2] J.L. Seran, A. Maillard, A. Fissolo, H. Touron, J. Royer, T. Martella, K. Erlich, H.J. Bergmann, in: Specialist Meeting on Cladding and Wrapper Materials, Obninsk, Russia, June 1992.
[3] V.D. Dmitriev, S.I. Porollo, V.S. Ageev, V.V. Romaneev, in: Proceedings of the International Conference on Radiation Materials Science, vol. 3, Alushta, 1990, p. 56.
[4] P.J. Maziasz, J. Nucl. Mater. 169 (1989) 95.
[5] P.J. Maziasz, J. Nucl. Mater. 108&109 (1982) 359.
[6] A.F. Rowcliffe, H. Lee, J. Nucl. Mater. 108&109 (1982) 306.
[7] F.A. Garner, J. Nucl. Mater. 122&123 (1984) 459.
[8] F.A. Garner, A.S. Kumar, in: F.A. Garner, N.H. Packan, A.S. Kumar (Eds.), Effects of Radiation on Materials: Thirteenth International Symposium (Part 1) Radiation-Induced Changes in Microstructure, ASTM STP 955, ASTM, Philadelphia, PA, 1987, p. 289.
[9] F.A. Garner, Materials Science and Technology: A Comprehensive Treatment, vol. 10A, VCH Publishers, 1994, p. 419.
[10] A.V. Tselischev, V.S. Ageev, Yu.P. Budanov, N.M. Mitrofanova, V.V. Novikov, in: Voprosy Atomnoi Nauki i Tekniki, vol. 1(66), 2006, p. 304.
[11] V.S. Ageev, V.M. Zyablov, E.A. Medvedeva, et al., in: Proceedings of International Conference on Radiation Materials Science, vol. 3, Alushta, 1990, p. 119.